Chemistry–A European Journal
Research Article
doi.org/10.1002/chem.202303874
Chemistry Europe
European Chemical Societies Publishing
www.chemeurj.org

Hot Paper

Photoinduced Dual C–F Bond Activation of Hexafluorobenzene Mediated by Boron Atom

Guohai Deng,*[a] Robert Medel,[a] Yan Lu,[a] and Sebastian Riedel*[a]

The reaction of laser-ablated boron atoms with hexafluorobenzene (C_6F_6) was investigated in neon and argon matrices, and the products are identified by matrix isolation infrared spectroscopy and quantum-chemical calculations. The reaction is triggered by a boron atom insertion into one C–F bond of hexafluorobenzene on annealing, forming a fluoropentafluorophenyl boryl radical (**A**). UV-Vis light irradiation of fluoropentafluorophenyl boryl radical causes generation of a 2-difluoroborotetrafluorophenyl radical (**B**) via a second C–F bond activation. A perfluoroborepinyl radical (**C**) is also observed upon deposition and under UV-Vis light irradiation. This finding reveals the new example of a dual C–F bond activation of hexafluorobenzene mediated by a nonmetal and provides a possible route for synthesis of new perfluorinated organo-boron compounds.

Introduction

Main Poly- and per-fluorinated organic molecules play important roles in materials science,[1] medicinal chemistry[2] and catalysis[3] because of their unique physical and chemical properties. Due to the strong and highly inert C–F bond,[4,5] the transformation of commercially available fluorinated aromatic building blocks into other fluorine-containing compounds are highly desirable but on the other hand also very challenging. Over the past decades, great contributions have been made to understand the reactivity of poly- and per-fluorinated aromatic molecules. The common approach to activate C–F bonds thus far relies on low-valent, low-coordinate transition-metal complexes by an oxidative addition.[6] Nevertheless, some main-group species are highly reactive and mimic the reactivity of transition-metal complexes as well, for instance, strong Lewis acids, frustrated Lewis pairs (FLPs),[7,8] N-heterocyclic carbene (NHC),[8] two-coordinate divalent Group 14 compounds,[9] base stabilized silylenes and germylenes,[10] N-heterocyclic aluminylenes,[11] Mg^{I}-Mg^{I} bonded compounds[12] and the N-heterocyclic olefin (NHO) 1,3,4,5-tetramethyl-2-methyleneimidazoline,[13] to name just a few. Very recently, Wu and co-workers have reported a site-selective C–F activation of polyfluoroarenes via electrophotocatalysis.[14] However, all the above-mentioned approaches are restricted to the activation of an single C–F bond, only very few transition-metal and boron compounds have been reported to be able to cleave a second C–F bond of polyfluorinated aromatic compounds.[15]

The atomic boron activation of C–H and C–C bonds of hydrocarbon to form organo-boron compounds is a fascinating subject of research and attracted considerable attention.[16–18,19,20] The boron atom can e.g. be inserted into the C–H bond of an acetylene molecule, forming the HBCCH molecule and the cyclic-HBC_2H radical in low-temperature inert matrices.[16,20] In addition, a cyclic-HBC_2BH diboron species is also generated by dual C–H bond activation of acetylene under UV-Vis light irradiation.[16] The products from the reaction of boron atoms with benzene were investigated by matrix-isolation spectroscopy in a solid neon matrices in conjunction with quantum-chemical calculations. Four BC_6H_6 isomers, namely, the η^2-(1,4) π adduct, the inserted borepinyl radical and the borole substituted vinyl radical as well as the final product 1-ethynyl-2-dihydro-1*H*-borole radical were characterized.[17] Although the reaction dynamics and kinetics of the reactions between atomic boron and hydrocarbons have been widely studied, investigations of elementary reactions of boron atoms with fluorinated organic molecules have remained scarce so far.[21] These studies are of significant interest due to C–F bonds having reverse polarity and higher bond energy in comparison to C–H bonds.[4] More importantly, these reactions can serve as the prototypical models to understand the mechanism of C–F bond activation of fluorinated molecules and the fluorine specific interactions.

Here, we report a joint matrix-isolation infrared spectroscopic and theoretical study on the reactions of boron atoms with hexafluorobenzene in solid neon and argon matrices. We show that besides the single C–F bond activation product fluoropentafluorophenyl boryl radical, and the C–C bond activation species perfluoroborepinyl radical, a 2-difluoroboryl-tetrafluorophenyl radical is also produced via dual C–F bond activation.

[a] *Dr. G. Deng, Dr. R. Medel, Y. Lu, Prof. Dr. S. Riedel*
Freie Universität Berlin
Institut für Chemie und Biochemie–Anorganische Chemie
Fabeckstrasse 34/36, 14195 Berlin (Germany)
s.riedel@fu-berlin
E-mail: ghdeng@zedat.fu-berlin.de

Supporting information for this article is available on the WWW under https://doi.org/10.1002/chem.202303874

Results and Discussion

The infrared spectra in the 1700–800 cm^{-1} region via the co-deposition of laser-ablated boron atoms from a ^{10}B-enriched (> 95 %) target and 0.05 % hexafluorobenzene (C_6F_6) in neon matrix are shown in Figure 1. In addition to the strong bands of hexafluorobenzene reactant, and the signals of the hexafluorobenzene anion (**1**, 1343.9, 889.2 and 856.9 cm^{-1})[22] as well as weak pentafluorophenyl radical (**2**, 1504.4 and 1060.5 cm^{-1})[22] absorptions, some new absorptions were detected. Absorptions of boron fluorides (BF, BF_2 and BF_3)[23] are barely observed, indicating little competition from fluorine abstraction reactions. These new product absorptions can be categorized into three groups based on their annealing and photochemical behaviors (labeled as **A**–**C** in Figure 1). Group **A** absorptions appeared on sample deposition and increased on annealing to 10 K. Two groups absorptions (**B** and **C**) markedly increased by the depletion of group **A** absorptions under UV-Vis light irradiation. Experiments were repeated using the natural abundance boron target under the same conditions to support products assignments. Similar experiments are repeated using 0.2 % C_6F_6 in Ar matrices. The infrared spectra in the selected region are shown in Figure S1 and corresponding difference infrared spectra in neon and argon are demonstrated in Figure 2 and Figure S2. The band positions are summarized in Table 1.

The group **A** absorptions at 1648.3, 1524.0, 1495.4, 1389.3, 1128.3, 993.3, 939.4, 777.7 and 623.3 cm^{-1} are assigned to different vibrational modes of the fluoropentafluorophenyl boryl radical. Apparently, the first three bands (1648.3, 1524.0 and 1495.4 cm^{-1}) with quite small ^{11}B shifts (0.4, 1.1 and 1.5 cm^{-1}) belong to the C–C stretching vibrations. The

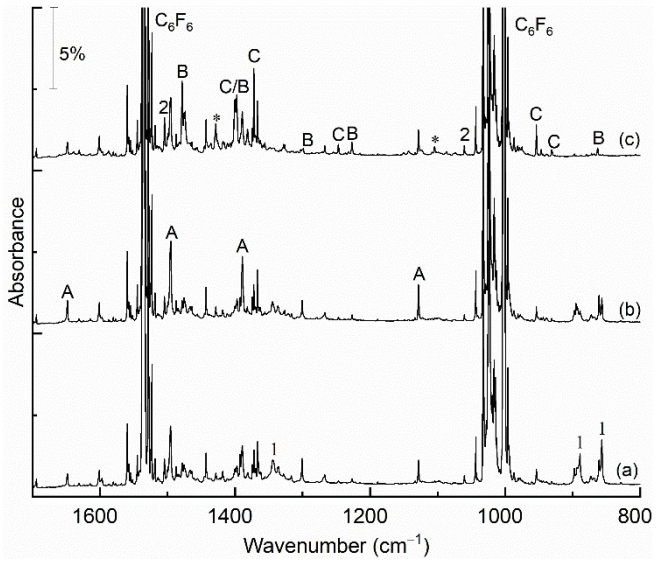

Figure 1. Infrared spectra in the 1700–800 cm^{-1} region from the co-deposition of ^{10}B-enriched boron atoms with 0.05 % C_6F_6 in neon. (a) After 30 min of sample deposition at 5 K, (b) after annealing to 10 K, and (c) after 10 min of $\lambda > 220$ nm UV-Vis light irradiation at 5 K. The bands of $C_6F_6^-$ (1), C_6F_5 (2), fluoropentafluorophenyl boryl radical (**A**), 2-difluoroboryl-tetrafluorophenyl radical (**B**), perfluoroborepinyl radical (**C**) and unidentified species (*) are labeled.

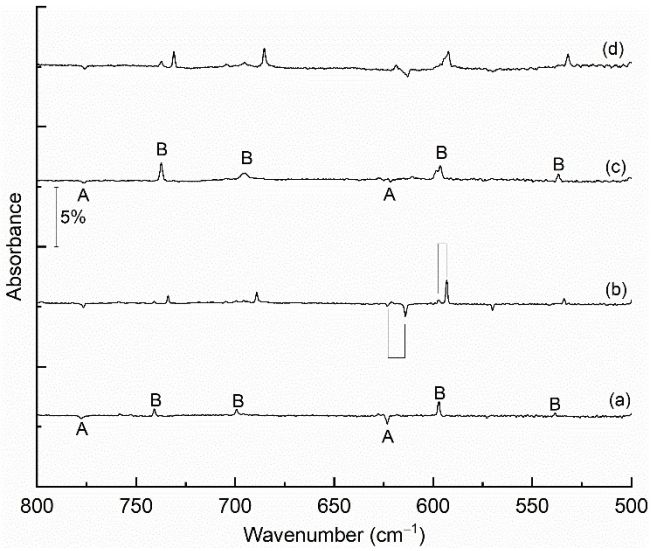

Figure 2. Infrared spectra in the 800–500 cm^{-1} region from the co-deposition of boron atoms with C_6F_6 in solid noble gas [spectra taken after 10 min $\lambda > 220$ nm UV-Vis light irradiation minus spectrum after annealing to 10 K (Ne) or 20 K (Ar)]: (a) $^{10}B + 0.05$ % C_6F_6 in neon; (b) $^{11}B + 0.05$ % C_6F_6 in neon; (c) $^{10}B + 0.2$ % C_6F_6 in argon; and (d) $^{11}B + 0.2$ % C_6F_6 in argon.

1389.3 cm^{-1} band, showing a very large boron isotopic shift (33.7 cm^{-1}) is the characteristic stretching vibration of the BF moiety in C_6F_5BF, which is red-shifted comparing to those of ^{10}BF (1412.2 cm^{-1}, N_2-matrix)[24] and $FBTiF_2$ (1404 cm^{-1}, Ar-matrix).[25] The bands at 939.4 and 623.3 cm^{-1} show large isotopic shifts (9.5 and 9.2 cm^{-1}), indicating that these absorptions can be mainly assigned to the B–C deformation modes. The last three absorptions (1128.3, 993.2 and 777.7 cm^{-1}) all exhibit small boron isotopic shifts (3.1, 0.9 and 0.9 cm^{-1}) and are mainly attributed to the C–F stretching vibrations and ring deformations.

Species **B** with absorptions at 1478.3, 1400.3, 1298.7, 1227.0, 1105.6, 863.0, 740.6, 699.2, 597.1 and 538.4 cm^{-1} are assigned to different vibrational modes of the 2-difluoroboryl-tetrafluorophenyl radical. The first three absorptions at 1478.3, 1400.3 and 1298.7 cm^{-1} with quite large boron isotopic shifts (21.5, 23.4 and 13.9 cm^{-1}) are ascribed to the mixed BF_2 antisymmetric or symmetric and C–C or C–F stretching vibrations. The bands at 740.6 and 699.2 cm^{-1}, that show large boron isotopic shifts, are assigned to the B–C bend vibrations. The other absorptions, that show relatively small isotopic shifts, are largely attributed to the C–F stretching vibrations or deformations and ring deformations or breathes.

Five absorptions at 1400.2, 1372.0, 1247.1, 953.8 and 930.7 cm^{-1} were observed for species **C**, which is assigned to the perfluoroborepinyl radical involving a seven-membered ring. The 1400.2 cm^{-1} absorption does not show a boron isotopic shift and mainly due to a C–C stretching mode. This band is very close to that of the parent borepinyl radical (1410.3 cm^{-1}, Ne-matrix).[17] The most intense absorption at 1372.0 cm^{-1} shows a large boron isotopic shift (13.4 cm^{-1}) implying that it largely due to the B–C stretching vibration. The other three absorptions at 1247.1, 953.8 and 930.7 cm^{-1}, that

Table 1. Comparison of the observed and calculated IR frequencies (cm^{-1}) and isotopic shifts (cm^{-1}) of the fluoropentafluorophenyl boryl radical (**A**), 2-difluoroboryl-tetrafluorophenyl radical (**B**) and perfluoroborepinyl radical (**C**) isomers.

	Exptl.						Calcd.[c]	
	Ne-matrix			Ar-matrix				
	^{10}B	^{11}B	$\Delta\nu$[b]	^{10}B	^{11}B	$\Delta\nu$	^{10}B	$\Delta\nu$[b]
A	1648.3	1647.9	0.4	1646.4	1646.3	0.1	1656 (119)	0.1
	1524.0	1522.9	1.1	1521.5	1521.1	0.4	1532 (129)	0.8
	1495.4	1493.9	1.5	1491.7	1490.2	1.5	1500 (586)	2.2
	_[a]	1385.5	_[a]	_[a]	_[a]	_[a]	1403 (297)	5.8
	1389.3	1355.6	33.7	1383.5	1349.9	33.6	1396 (226)	31.6
	1128.3	1125.2	3.1	1125.4	1122.5	2.9	1136 (148)	3.1
	993.2	992.3	0.9	991.0	990.2	0.8	1004 (188)	1.2
	939.4	929.9	9.5	_[a]	_[a]	_[a]	944 (30)	9.9
	777.7	776.8	0.9	776.7	775.8	0.9	784 (13)	0.9
	623.3	614.1	9.2	621.2	613.5	8.7	624 (34)	9.8
B	1478.3	1456.8	21.5	1472.1	1451.7	20.4	1480 (623)	18.2
	1400.3	1376.9	23.4	1396.0	1373.7	22.3	1401 (746)	22.4
	1298.7	1284.8	13.9	1297.2	1283.7	13.5	1292 (104)	11.3
	1227.0	1221.2	5.8	1223.1	1217.8	5.3	1253 (64)	6.3
	1105.6	1105.4	0.2	1102.3	1102.0	0.3	1111 (45)	1.4
	863.0	862.1	0.9	862.6	862.0	0.6	868 (49)	0.0
	740.6	734.0	6.6	737.3	730.9	6.4	764 (13)	3.7
	699.2	689.3	9.9	695.4	685.6	9.8	716 (26)	11.1
	597.1	593.2	3.9	596.5	592.2	4.3	598 (37)	4.3
	538.4	534.0	4.4	536.9	532.1	4.8	550 (11)	5.4
C	1400.2	1400.2	0.0	1396.3	1396.3	0.0	1389 (261)	0.0
	1372.0	1358.6	13.4	1367.6	1354.6	13.0	1373 (729)	14.0
	1247.1	1246.7	0.4	_[a]	_[a]	_[a]	1227 (133)	1.0
	953.8	946.1	7.7	951.2	943.8	7.4	993 (156)	4.0
	930.7	926.9	3.8	928.2	_[a]	_[a]	960 (252)	6.5

[a] Absorption bands not observed, or overlapped. [b] The boron-11, isotopic shift is labeled as $\Delta\nu$. [c] Harmonic frequencies calculated at the B3LYP/aug-cc-pVTZ level is listed with intensities ($km\,mol^{-1}$) in parentheses. The complete set of vibrational frequencies are provided in Supporting Information Table S1–S3.

show small to medium boron-11 isotopic shifts (0.4, 7.7 and 3.8 cm^{-1}), are mainly attributed to the C–F stretching vibration and seven-membered ring deformations.

In order to identify the structures of observed products and understand the formation mechanism, the density functional theory calculations were carried out. Figure 3 shows the calculated structures of the experimentally detected species **A**–**C** at the B3LYP/aug-cc-pVTZ level. All three products are predicted to have doublet electronic ground states. The species **A** and **B** both have a $^2A'$ ground state with C_s symmetry. The B–C and B–F bonds distance (1.554 and 1.309 Å) in species **A** are predicted to be slightly shorter than those in species **B** (1.556 and 1.319/1.322 Å). The bond angle of F–B–C in species **A** is 123.6°, which is slightly larger than that in species **B** (119.8/122.4°). The unpaired electron is mainly located on either the boron atom (**A**) or the carbon atom (**B**) (Figure 4). The shapes of selected highest-lying occupied molecular orbitals (HOMO) of species **A**, **B** and **C** are shown in Figure S3. Therefore, the species **A** and **B** are boron-center radical and difluoroboryl-substituted tetrafluorophenyl radical, respectively.

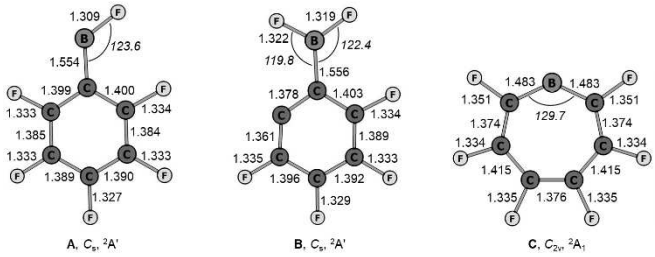

Figure 3. Calculated structures (bond lengths in angstroms and bond angles in degrees) of fluoropentafluorophenyl boryl radical (**A**), 2-difluoroboryl-tetrafluorophenyl radical (**B**) and perfluoroborepinyl radical (**C**) at the B3LYP/aug-cc-pVTZ level.

Species **C** is predicted to have a planar structure with a C_{2v} symmetry involving a seven-membered ring. The nonplanar C_2 symmetry structure (Figure S4) has a very close energy (<

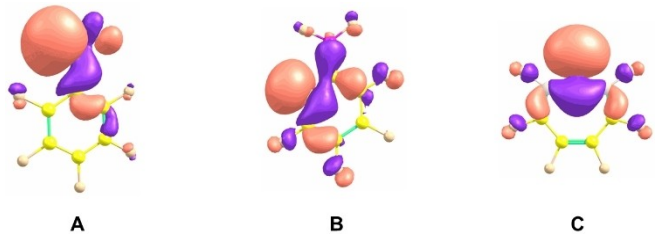

Figure 4. Shapes of the SOMO of experimentally observed fluoropentafluorophenyl boryl radical (**A**), 2-difluoroboryl-tetrafluorophenyl radical (**B**) and perfluoroborepinyl radical (**C**) plotted with isosurfaces = 0.03 a.u at the B3LYP/aug-cc-pVTZ level.

0.1 kcal mol^{-1}) with the C_{2v} structure at the CCSD(T)/cc-pVTZ//B3LYP/aug-cc-pVTZ level. The bond angle of the C–B–C subunit is 129.7° which is much smaller than that in the parent borepinyl radical (151.7°) at the same level of theory. The C–B bond distance (1.483 Å) in species **C** is longer than those previous report of the carbon–boron bond distance in borepinyl radical (1.439 Å)[17] and the H_2CBCH_2 molecule (1.425 Å)[18] at the same level. The computed spin density is largely located on the boron atom (0.851e) (Figure S5). This is the driving force for adopting the C_{2v} symmetry structure differing to the H-analogous borepinyl radical, which was identified to have a C_2 symmetric structure because of the unpaired electron mainly at the CBC moiety.[17] The difference between the perfluoroborepinyl (C_{2v}) and the borepinyl (C_2) radicals is mainly due to the electronegativity of fluorine being much higher than that of hydrogen. The high electronegativity decreases the spin density on the carbon atoms, indicating a type of fluorine specific interactions.

The computed vibrational frequencies, intensities, and boron isotopic shifts of experimentally detected modes for the three $^{10}BC_6F_6$ isomers are compared with the experimental values in neon and argon matrices in Table 1. The complete computed vibrational frequencies, intensities, and boron isotopic shifts are shown in Table S1–S3. For species **A**, a computed strong absorption at 1403 cm^{-1} with 297 km mol^{-1} IR intensity was not observed, likely owing to overlapping with the absorption at 1389.3 cm^{-1}. Only the ^{11}B isotopolog band was detected at 1385.5 cm^{-1}. For species **B**, a predicted strong absorption at 1025 cm^{-1} with 158 km mol^{-1} IR intensity (Table S2) was not identified due to overlapping with the very strong IR bands of C_6F_6 in this region. For species **C**, two bands at 1400.2 and 1247.1 cm^{-1} are higher than the theoretically predicted wavenumber at the B3LYP/aug-cc-pVTZ level, but close to the calculated one using double-hybrid DFT (B2PLYPD3/aug-cc-pVTZ) method (Table S3). Other predicted absorption bands for species **A**, **B** and **C** are not observed due to their low intensity or too low wavenumbers which are outside the measured spectral range (4000–450 cm^{-1}). The good agreement between the computed frequencies and boron isotopic shifts and experimental values strongly supports the vibrational assignments and the identification of these perfluorinated organo-boron compounds.

The experimental results clearly suggest that the absorptions of the fluoropentafluorophenyl boryl radical (**A**) increase on annealing, indicating that the ground-state boron atom can insert into the C–F bond of hexafluorobenzene at cryogenic temperature. As shown in Figure 5, the detailed potential energy profile for the reaction of the ground-state B (^2P) atoms with hexafluorobenzene to form **A**, **B** and **C** were calculated at the CCSD(T)/cc-pVTZ//B3LYP/aug-cc-pVTZ level. Other possible intermediates that can be accessed on excited-state surfaces are not considered. The structures of corresponding intermediates and transition states are displayed in Figure S6. In contrast with the boron atom reaction with benzene forming the η^2-(1,4) BC_6H_6 π adducts,[17] the boron atom insertion into the C–F bond in the reaction with hexafluorobenzene produce the fluoropentafluorophenyl boryl radical (**A**) on annealing. This insertion reaction is barrierless and involves an exothermic energy change of 120.8 kcal mol^{-1}, which is significantly larger than the atomic boron insertion into the C–H bond of benzene to yield the phenylboryl radical (61.2 kcal mol^{-1}) at CCSD(T)/cc-pVTZ//B3LYP/6-311 + G** level.[26] The difference in energy between the two reactions are mainly owing to the formation of a very strong B–F bond. Species **A** rearranges to the 2-difluoroboryl-tetrafluorophenyl radical (**B**) via a transition state (TS1) located only 34 kcal mol^{-1} above the species **A** structure. This rearrangement reaction is calculated to be exothermic by 50.5 kcal mol^{-1}.

The rearrangement reaction from the fluoropentafluorophenyl boryl radical (**A**) to the perfluoroborepinyl radical (**C**) is quite complicated. The conversion of species **A** to product **C** is endothermic by 57.7 kcal mol^{-1} and proceeds via two intermediates (**I1** and **I2**). Species **A** rearranges to the intermediate **I1** via a transition state (TS2) located only 35.4 kcal mol^{-1} above the species **A** structure. This transition state (TS2) barrier is energetically very close to the one for TS1 (34 kcal mol^{-1}). However, this intermediate **I1** was not detected in the experiment. Theoretical prediction of the infrared frequencies and

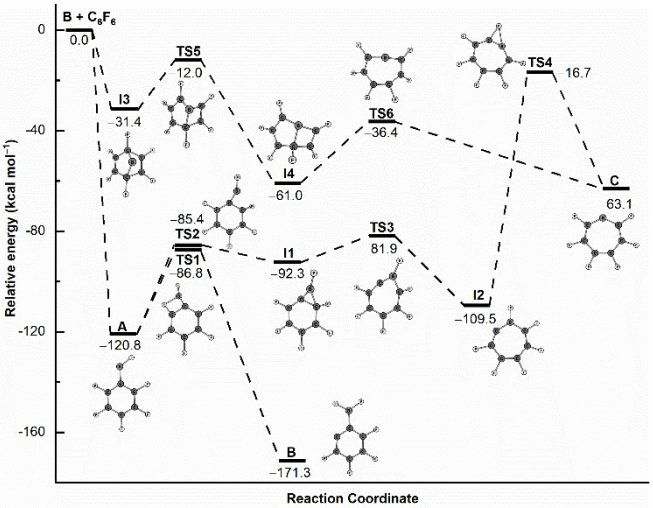

Figure 5. Calculated potential energy profile for the reaction of the ground-state B(^2P) atom with hexafluorobenzene (C_6F_6) at the CCSD(T)/cc-pVTZ//B3LYP/aug-cc-pVTZ level. The energies are in kcal mol^{-1} and are corrected with zero-point energy.

intensities of **I1** are shown in Table S4. The intermediate **I1** is barely unstable and will likely further isomerize to the intermediate **I2** via a transition state (TS3) located only 10.4 kcal mol^{-1} above the species **I1** structure. This reaction is exothermic by 17.2 kcal mol^{-1}. The low energy barrier may be the reason that the species **I1** was not detected experimentally. The calculated infrared frequencies and intensities of **I2** are also given in Table S4. Although no experimental infrared absorption band could be assigned to **I1** or **I2**, the possibility of forming **I1** and **I2** from product **A** could not be excluded owing to the low energy barrier. The F atom transfer process from **I2** to products **C** is predicted to be endothermic by 46.4 kcal mol^{-1} and requires high activation energy (102.8 kcal mol^{-1}). This isomerization process involves B–F bond cleavage and proceeds only under UV-Vis light ($\lambda > 220$ nm) irradiation, during which some excited states may be involved.

Considering the formation of borepinyl radical from the reaction of boron and benzene,[17] the perfluoroborepinyl radical (**C**) can also be generated from the C–C bond insertion reaction. The formation of product **C** from starting reactants ($B + C_6F_6$) is exothermic and proceeds via two intermediates (**I3** and **I4**). The η^2 adduct **I3** is predicted to be 31.4 kcal mol^{-1} lower than the reactants ($B + C_6F_6$), but 89.4 kcal mol^{-1} higher than species **A**. The intermediate **I3** can isomerize to intermediate **I4** via a transition states TS5 through C–C bond cleavage. The barrier for TS5 lies 12.0 kcal mol^{-1} below the energy of ground-state reactants and is about 19.4 kcal mol^{-1} above the η^2 adduct (**I3**). The isomerization reaction from intermediate **I4** to the perfluoroborepinyl radical (**C**) via C–B bond cleavage is calculated to proceed through a transition state (TS6) lying 14.6 kcal mol^{-1} above structure **I4**. The overall C–C bond insertion reaction in generating perfluoroborepinyl radical **C** is computed to be exothermic by 63.1 kcal mol^{-1}. Although the H-analogue of intermediate **I4** has been observed in the reaction of benzene with atomic boron,[17] no absorption can be assigned to the intermediates **I3** and **I4** (Table S4). Given that the highest transition state (TS4) lies 12.0 kcal mol^{-1} lower in energy than the ground-state reactants $B + C_6F_6$, the isomerization and C–C bond insertion reactions are both thermodynamically favorable and kinetically facile.

Conclusions

The reactions of atomic boron with hexafluorobenzene molecules in solid neon and argon matrices were investigated by matrix-isolated IR spectroscopy and quantum-chemical calculations. The results clearly show that the ground-state boron atoms react with hexafluorobenzene to form the C–F bond-inserted fluoropentafluorophenyl boryl radical (**A**) on annealing in solid neon and argon. The fluoropentafluorophenyl boryl radical (**A**) can further rearrange to the more stable 2-difluoroboryl-tetrafluorophenyl radical (**B**) via ortho-F atom migration under UV-Vis light excitation. A perfluoroborepinyl radical (**C**) involving a seven-membered ring was also detected under UV-Vis light irradiation. The generation of 2-difluoroboryl-tetrafluorophenyl radical suggest that the second C–F bond of hexfluorobenzene is activated in the reaction with atomic boron. This finding reveals the new example of a dual C–F bond activation of hexafluorobenzene, which provides a possible new reaction route for metal-free C–F bond activation of hexafluorobenzene in producing new perfluorinated organoboron compounds.

Acknowledgements

We gratefully acknowledge the Zentraleinrichtung für Datenverarbeitung (ZEDAT) of the Freie Universität Berlin for the allocation of computing resources. We thank the CRC 1349 (SFB 1349) Fluorine Specific Interactions – Project-ID 387284271 – for continuous support. G. Deng thanks the Alexander von Humboldt Foundation (AvH) for a research scholarship. Open Access funding enabled and organized by Projekt DEAL.

Conflict of Interests

The authors declare no conflict of interest.

Data Availability Statement

The data that support the findings of this study are available from the corresponding author upon reasonable request.

Keywords: C–F bond activation · Boron · Matrix-isolation Infrared spectroscopy · Quantum-chemical calculations

[1] a) Z. Chu, S. Seeger, *Chem. Soc. Rev.* **2014**, *43*, 2784–2798; b) M. L. Tang, Z. Bao, *Chem. Mater.* **2011**, *23*, 446–455; c) R. Berger, G. Resnati, P. Metrangolo, E. Weber, J. Hulliger, *Chem. Soc. Rev.* **2011**, *40*, 3496–3508.
[2] a) B. M. Johnson, Y.-Z. Shu, X. Zhuo, N. A. Meanwell, *J. Med. Chem.* **2020**, *63*, 6315–6386; b) Y. Zhou, J. Wang, Z. Gu, S. Wang, W. Zhu, J. L. Aceña, V. A. Soloshonok, K. Izawa, H. Liu, *Chem. Rev.* **2016**, *116*, 422–518; c) S. Purser, P. R. Moore, S. Swallow, V. Gouverneur, *Chem. Soc. Rev.* **2008**, *37*, 320–330.
[3] a) Z.-Z. Xie, Y. Zheng, C.-Pi. Yuan, J.-P. Guan, Z.-P. Ye, J.-A. Xiao, H.-Y. Xiang, K. Chen, X.-Q. Chen, H. Yang, *Angew. Chem. Int. Ed.* **2022**, *61*, e2022110; *Angew. Chem.* **2022**, *134*, e2022110; b) W. G. Xu, H. M. Jiang, J. Leng, H.-W. Ong, J. Wu, *Angew. Chem. Int. Ed.* **2020**, *59*,4009–4016; *Angew. Chem.* **2020**, *132*, 4038–4045; c) R. Shintani, N. Misawa, T. Tsuda, R. Iino, M. Fujii, K. Yamashita, K. Nozaki, *J. Am. Chem. Soc.* **2017**, *139*, 3861–3867; d) T. Ritter, M. W. Day, R. H. Grubbs, *J. Am. Chem. Soc.* **2006**, *128*, 11768–11769.
[4] D. O'Hagan, *Chem. Soc. Rev.* **2008**, *37*, 308–319.
[5] S. J. Blanksby, G. B. Ellison, *Acc. Chem. Res.* **2003**, *36*, 255–263.
[6] a) T. Ahrens, J. Kohlmann, M. Ahrens, T. Braun, *Chem. Rev.* **2015**, *115*, 931–972; b) H. Amii, K. Uneyama, *Chem. Rev.* **2009**, *109*, 2119–2183; c) T. Schaub, M. Backes, U. Radius, *J. Am. Chem. Soc.* **2006**, *128*, 15964–15964.
[7] T. Stahl, H. F. T. Klare, M. Oestreich, *ACS Catal.* **2013**, *3*, 1578–1587.
[8] C. B. Caputo, D. W. Stephan, *Organometallics* **2012**, *31*, 27–30.
[9] M. Pait, G. Kundu, S. Tothadi, S. Karak, S. Jain, K. Vanka, S. S. Sen, *Angew. Chem. Int. Ed.* **2019**, *58*, 2804–2808; *Angew. Chem.* **2019**, *131*, 2830–2834.
[10] A. Jana, P. P. Samuel, G. Tavcar, H. W. Roesky, C. Schulzke, *J. Am. Chem. Soc.* **2010**, *132*, 10164–10170.
[11] M. R. Crimmin, M. J. Butler, A. J. P. White, *Chem. Commun.* **2015**, *51*, 15994–15996.
[12] C. Bakewell, A. J. P. White, M. R. Crimmin, *J. Am. Chem. Soc.* **2016**, *138*, 12763–12766.

[13] D. Mandal, S. Chandra, N. I. Neuman, A. Mahata, A. Sarkar, A. Kundu, S. Anga, H. Rawat, C. Schulzke, K. R. Mote, B. Sarkar, V. Chandrasekhar, A. Jana, *Chem. Eur. J.* **2020**, *26*, 5951–5955.
[14] Y.-J. Chen, W.-H. Deng, J.-D. Guo, R.-N. Ci, C. Zhou, B. Chen, X.-B. Li, X.-N. Guo, R.-Z. Liao, C.-H. Tung, L.-Z. Wu, *J. Am. Chem. Soc.* **2022**, *144*, 17261–17268.
[15] a) M. Arisawa, T. Suzuki, T. Ishikawa, M. Yamaguchi, *J. Am. Chem. Soc.* **2008**, *130*, 12214–12215; b) H. Guo, F. Kong, K. Kanno, J. He, K. Nakajima, T. Takahashi, *Organometallics* **2006**, *25*, 2045–2048; c) T. J. Korn, M. A. Schade, S. Wirth, P. Knochel, *Org. Lett.* **2006**, *8*, 725–728; d) T. Saeki, Y. Takashima, K. Tamao, *Synlett* **2005**, 11, 1771–1774; e) H. Budy, S. E. Prey, C. D. Buch, M. Bolte, H.-W. Lerner, M. Wagner, *Chem. Commun.* **2022**, *58*, 254–257; f) J. Landmann, P. T. Hennig, N. V. Ignat'ev, M. Finze, *Chem. Sci.* **2017**, *8*, 5962–5968.
[16] J. Jian, W. Li, X. Wu, M. Zhou, *Chem. Sci.* **2017**, *8*, 4443–4449.
[17] J. Jian, X. Wu, M. Chen, M. Zhou, *J. Am. Chem. Soc.* **2020**, *142*, 10079–10086.
[18] J. Jian, H. Lin, M. Luo, M. Chen, M. Zhou, *Angew. Chem. Int. Ed.* **2016**, *55*, 8371–8374; *Angew. Chem.* **2016**, *128*, 8511–8514.
[19] a) N. Balucani, F. Zhang, R. I. Kaiser, *Chem. Rev.* **2010**, *110*, 5107–5127; b) D. V. Lanzisera, P. Hassanzadeh, Y. Hannachi, L. Andrews, *J. Am. Chem. Soc.* **1997**, *119*, 12402–12403.
[20] J. M. L. Martin, P. R. Taylor, P. Hassanzadeh, L. Andrews, *J. Am. Chem. Soc.* **1993**, *115*, 2510–2511.
[21] D. V. Lanzisera, L. Andrews, *J. Phys. Chem. A* **2000**, *104*, 9295–9301.
[22] S.-L. Chou, S.-Y. Lin, M.-Y. Lin, Y.-J. Wu, *Spectrochim. Acta Part A* **2021**, *252*, 119524.
[23] X.-F. Wang, L. Andrews, *J. Am. Chem. Soc.* **2011**, *133*, 3768–3771.
[24] B. Xu, H. Beckers, H. Ye, Y. Lu, J. Cheng, X. Wang, S. Riedel, *Angew. Chem. Int. Ed.* **2021**, *60*, 17205–17210; *Angew. Chem.* **2021**, *133*, 17342–17347.
[25] X. Wang, B. O. Roos, L. Andrews, *Angew. Chem. Int. Ed.* **2010**, *49*, 157–160; *Angew. Chem.* **2010**, *122*, 161–164.
[26] H. F. Bettinger, R. I. Kaiser, *J. Phys. Chem. A* **2004**, *108*, 4576–4586.

Manuscript received: November 21, 2023
Accepted manuscript online: January 9, 2024
Version of record online: January 23, 2024